Available online at www.sciencedirect.com
ScienceDirect
Journal of Physics and Chemistry of Solids 68 (2007) 1571–1582
JOURNAL OF PHYSICS AND CHEMISTRY OF SOLIDS
www.elsevier.com/locate/jpcs

Electrical and optical properties of Jäger-nickel (II)-based molecular-material thin films prepared by the vacuum thermal evaporation technique

O.G. Morales-Saavedra[a], M.E. Sánchez Vergara[b,*], A. Ortiz Rebollo[c], R. Ortega-Martínez[a]

[a]*Centro de Ciencias Aplicadas y Desarrollo Tecnológico, CCADET-UNAM, Universidad Nacional Autónoma de México, A.P. 70-186, Coyoacán, 04510 México, DF, México*

[b]*Departamento de Ingeniería Mecatrónica, Escuela de Ingeniería, Universidad Anahuac del Norte, Avenida Lomas de la Anahuac s/n, Col. Lomas Anahuac, 52786 Huixquilucan, Estado de México, México*

[c]*Instituto de Investigaciones en Materiales, IIM-UNAM. Universidad Nacional Autónoma de México, A.P. 70-360, Coyoacán, 04510 México, DF, México*

Received 22 December 2006; received in revised form 22 March 2007; accepted 22 March 2007

Abstract

Semiconductor molecular-material thin films of [6,13-Ac_2-5,14-Me_2-[14]-4,6,11,13-tetraenato-1,4,8,11-N_4] and the bidentate amines 1,4-diaminebutane, 1,12-diaminedodecane and 2,6-diamineanthraquinone have been prepared by vacuum thermal evaporation on corning glass substrates and crystalline silicon wafers. The films thus obtained were characterized by infrared (FTIR), ultraviolet–visible (UV–VIS) and photoluminescence (PL) spectroscopies. The surface morphology, thickness and structure of these films were analyzed by atomic force microscopy (AFM), ellipsometry and X-ray diffraction (XRD), respectively. IR spectroscopy showed that the molecular-material thin films exhibit the same intra-molecular bonds as the original compounds, which suggests that the thermal evaporation process does not significantly alter their bonds. The effect of temperature on conductivity was also measured in these samples; it was found that the temperature-dependent electric current is always higher for the voluminous amines with large molecular weights and suggests a semiconductor behavior with conductivities in the order of 10^{-6}–$10^{-1}\,\Omega^{-1}\,cm^{-1}$. Finally, the optical band gap (E_g) and cubic $\chi^{(3)}$ non-linear optical (NLO) properties of these amorphous molecular complexes were also evaluated from optical absorption and optical third harmonic generation (THG) measurements, respectively.

Keywords: A. Thin films; B. Chemical synthesis; D. Electrical properties; D. Optical properties; D. Semiconductivity

1. Introduction

In the last few years, there has been an increasing interest in molecular materials because of their peculiar electric and optical properties, which may lead to electronic and opto-electronic device applications [1–3]. It is difficult to envision a technological breakthrough while using them in the usual, single-crystalline form, but the thin-film production of such materials offers an attractive alternative [4–7]. Recent research work has been oriented to the formation and characterization of molecular-material thin films with potential photonic, opto-electronic or electrode-device applications [8,9]. It is well known that the properties of such thin films strongly depend on their microstructure [10]. A regular stacking of molecules such as is found in molecular materials may permit the formation of semiconducting, conducting or superconducting thin films. Their highly anisotropic conductivity almost reaches metallic values along a preferred direction defined by their structural configuration. This phenomenon arises from a great number of long and parallel chains or molecular stacks along which conduction seems to occur. Therefore, in order to describe the relationship between the electrical properties and physical configuration of the thin films, it is necessary to obtain such systems with a well-defined microstructure [10].

*Corresponding author. Tel.: +52 55 56270210x8236; fax: +52 55 56270210x823.
E-mail address: elena.sanchez@anahuac.mx (M.E. Sánchez Vergara).

0022-3697/$ - see front matter © 2007 Elsevier Ltd. All rights reserved.
doi:10.1016/j.jpcs.2007.03.040

In order to create the molecular-material thin films reported in this paper, we used Jäger-type compounds forming stable complexes with a metallic ion. Jäger compounds show good overall optical and electronic properties when forming thin films. This is essential to achieve successful studies concerning charge transfer processes occurring in several physical and chemical material phenomena. Synthesis of molecular materials was carried out from Jäger nickel (II) compounds leasing in the carbonyl and the subsequent addition in the leased zone of bidentate amines: 1,4-diaminebutane, 1,12-diaminedodecane and 2,6- diamineanthraquinone.

In this work, thermal evaporation has been employed to grow the new Jäger-nickel (II)-based thin films. As observed in amorphous inorganic semiconductors, loss of periodicity and crystalline structure results in the localization of electronic wave functions and tail formation in the density of states which extends into the forbidden energy gap at the valence and conduction band edges. Electrical conduction can then be explained by means of band theory and a hopping model establishing a mobility edge for the charge carriers. Under this context, the existence of charge carriers in these amorphous structures may lead to the observation of interesting linear and non-linear optical (NLO) effects too, like the optical third harmonic generation (THG) and non-linear refraction. We therefore performed several types of physical characterizations in order to investigate the developed Jäger-based compounds, including the structural, morphological, electrical, linear and non-linear optical properties of these complex molecular systems.

2. Experimental section

2.1. Starting materials and chemicals

Molecular materials were synthetized from the precursor $[Ni(C_{18}H_{28}N_4O_2)](PF_6)_2$: [6,13-$Ac_2$-5,14-$Me_2$-[14]-4,6,11,13-tetraenato-1,4,8,11-N_4] macrocycle leased in the carbonyl, as in the technique proposed by Corfield et al. [11], in order to generate methoxy groups at the same site, and treat them later with 1,4-diaminebutane, 1,12-diaminedodecane and 2,6-diamine anthraquinone bidentated amines, with the purpose of substituting the methoxy groups with amino groups.

Synthesis of $[Ni(C_{17}H_{25}N_4ONH(CH_2)_4NH_2)](PF_6)_2$ *(compound* 1a*)*: 1.0 g (2.6 mmol) of [6,13-Ac_2-5,14-Me_2-[14]-4,6,11,13-tetraenate-1,4,8,11-N_4] complex dissolved in 40 ml of acetonitrile and treated later with 5 ml 1,4 diaminebutane (in excess). The solution was concentrated and refrigerated to achieve the crystallization of the product. The solid was filtered off, washed with absolute methanol and vacuum-dried. The product was recrystallized in 1:1 acetonitrile-methanol. Yield 68% (0.89 g). (Found: C, 50.50; H, 8.06; N, 16.66. Calcd.: C, 50.30; H, 8.38; N, 16.77.).

Synthesis of $[Ni(C_{17}H_{25}N_4ONH(CH_2)_{12}NH_2)](PF_6)_2$ *(compound 1b):* 1.0 g (2.6 mmol) of [6,13-Ac_2-5,14-Me_2-[14]-4,6,11,13-tetraenate-1,4,8,11-N_4] complex dissolved in 40 ml of acetonitrile and treated with 1.04 g of 1,12-diaminododecane (in excess), previously dissolved in 40 ml of acetonitrile. This solution is concentrated and refrigerated for product crystallization. The solid was filtered off, washed with absolute methanol and vacuum-dried. The product was recrystallized in 1:1 acetonitrile–methanol. Yield 76.3% (1.44 g). (Found: C, 50.47; H, 9.20; N, 12.57. Calcd.: C, 50.66; H, 9.61; N, 12.22.).

Synthesis of $[Ni(C_{17}H_{25}N_4O(C_{14}H_{10}N_2O_2))](PF_6)_2$ *(compound 1c):* 1.0 g (2.6 mmol) of [6,13-Ac_2-5,14-Me_2-[14]-4,6,11,13-tetraenate-1,4,8,11-N_4] complex dissolved in 40 ml of acetonitrile. Afterwards, 0.6 mL (4.3 mmol) of triethylamine, and then 1.24 g of 2,6-diamineanthraquinone (in excess, previously dissolved in 40 ml of acetonitrile) were added, respectively. This solution was concentrated and refrigerated for product crystallization. The solid was filtered off, washed with absolute methanol and vacuum-dried. The product was recrystallized in 1:1 acetonitrile–methanol. Yield 77.8% (1.62 g). (Found: C, 50.15; H, 6.28; N, 11.23. Calcd.: C, 50.20; H, 6.75; N, 11.34.).

The synthesis route, starting from the precursor sample up to the generation of compounds 1a–1c, is schematically shown in Fig. 1.

2.2. Thin-film deposition

Thin film deposition of compounds 1a–c—$[Ni(C_{17}H_{25}N_4ONH(CH_2)_4NH_2)](PF_6)_2$, $[Ni(C_{17}H_{25}N_4ONH(CH_2)_{12}NH_2)](PF_6)_2$ and $[Ni(C_{17}H_{25}N_4O(C_{14}H_{10}N_2O_2))](PF_6)_2$—was carried out by vacuum thermal evaporation onto Corning 7059 glass slices and (1 0 0) single-crystalline silicon (c-Si), 200 Ω cm wafers. The substrate temperatures were kept at 298 K during deposition. The Corning 7059 substrates were ultrasonically degreased in warm ethanol and dried in a nitrogen atmosphere. The substrates underwent chemical etching with a *p* solution (10 ml HF, 15 ml HNO_3, and 300 ml H_2O) in order to remove the native oxide from the c-Si surface. To prevent the powder products from condensing on the surface of the substrate, the evaporation source was a molybdenum boat with two grids. The temperature in the boat was set to 453 K during evaporation and was monitored with a chromel–alumel thermocouple. It should be remarked that the synthesized compounds sublimate. The temperature through the molybdenum boat was slowly increased to 453 K, below the first significant signal change observed in the thermo-gravimetric analysis thermogram, in order to prevent thermal decomposition of the compound and to identify the phase changes (evaporation, sublimation). All samples were obtained using the same deposition system, with the crucible and substrates disposed in the same geometry. The base pressure in the deposition chamber before thin-film deposition and the amount of mass inside the crucible were the same in all cases. In spite of these similarities, significant differences in the thickness of

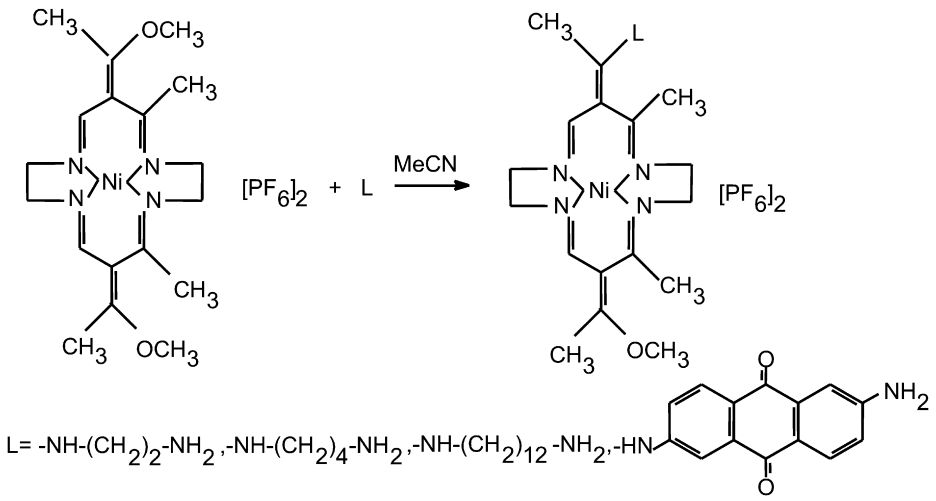

Fig. 1. Chemical structures of the synthesized molecular materials, obtained from Jäger nickel (II) compounds (L represents the bidentate amine).

deposited films were detected, which may be related to differences in the sublimation processes for the compounds used (see next sections).

2.3. Thin-film characterization

(i) The surface morphology of films deposited on Corning-7059 glass slices was analyzed by Atomic Force Microscopy (AFM) (Park AutoProbe CP equipment). Image acquisition was performed in contact mode with an interaction force applied between the sample and the AFM-tip of 1.5 nN. The AFM system was equipped with a SiN sharpened Microlever^{TM} tip with a typical force constant of $0.05\,N\,m^{-1}$ and a resonant frequency of 22 KHz specifying the mechanical characteristics of the cantilever. (ii) The thin films were analyzed by means of infrared spectroscopy (FTIR) and were recorded with a Nicolet 5-Mx FTIR spectrophotometer with a resolution of $4\,cm^{-1}$. (iii) Film thickness was determined by ellipsometry using a Gaetner L117 variable-angle manual ellipsometer, equipped with a helium–neon laser as a light source ($\lambda = 632.8$ nm, $\varnothing = 1$ mm at 1 mW). The incidence angle was 70°. The infrared and ellipsometric measurements were carried out in films deposited onto c-Si substrates. (iv) The electric conductivity of the films was studied by means of a four-point probe; for these measurements, the substrates were Corning 7059 glass slices coated with four metallic strips that acted as electrodes. The strips were deposited by thermal evaporation. In order to get an ohmic contact with the deposited films, the electrodes were made from gold or silver. Electric current as a function of temperature was measured with an applied voltage of 100 V in the ohmic regime, using a Keithley 230 programmable voltage source and a Keithley 485 peak-ammeter coupled to an HP3421 data collector. (v) The optical absorption spectra of films deposited on Corning 7059 glass slices were obtained within the 200–1100 nm spectral range using a double beam Shimadzu UV–VIS spectrophotometer. (vi) Photoluminescent (PL) spectra of films deposited on Corning 7059 glass slices were obtained from 250 to 700 nm using an excitation line at $\lambda_{ex} = 250$ nm with a FluoroMax-3, Jobin-Yvon-Horiba fluorimeter equipment. (vii) Structural studies were performed in these films through XRD by the $\theta-2\theta$ technique with a Siemens D5000-diffractometer using Cu $K\alpha_1$ ($\lambda = 0.15405$ nm) radiation. Finally, the developed thin films deposited on Corning 7059 glass slices were also considered as active media for cubic $\chi^{(3)}$-NLO effects like THG. The THG experimental device is schematically shown in Fig. 2, where a commercial Q-switched Nd:YAG laser system (Surelite II from Continuum, $\lambda_\omega = 1064$ nm, repetition rate of 10 Hz and a pulse width of $\tau = 12$ ns) was implemented to provide the fundamental wave. Pulse powers of ~150 μJ were filtered in order to irradiate the samples by means of a $f = 50$ mm focusing lens, thus peak irradiances in the order of $80\,MW\,cm^{-2}$ were achieved at the focal spot on the molecular thin films. This value was slightly below the energy damage threshold supported by the samples under strong focused laser beam irradiation. The polarization of the fundamental beam (S or P polarizing geometry) was selected by means of an IR-coated Glan-laser polarizer and a $\lambda/2$-quarz-retarder. A second polarizer was used as analyzer allowing the characterization of the THG-signals. The second harmonic waves (at $\lambda_{3\omega} = 355$ nm) were detected by a sensitive photomultiplier tube (HAMAMATSU R-928) placed behind interferential optical filters (centered at 355 ± 5 nm). The THG-device was calibrated by means of a fused silica plate ($\chi^{(3)} = 3.11 \times 10^{-14}$ esu at $\lambda_\omega = 1064$ nm), which is commonly used as a NLO-reference standard via the Maker-Fringes method [12–18].

3. Results and discussion

3.1. Thin-film morphology and XRD studies

The variations in the microscopic morphology and roughness of the films were examined by atomic force

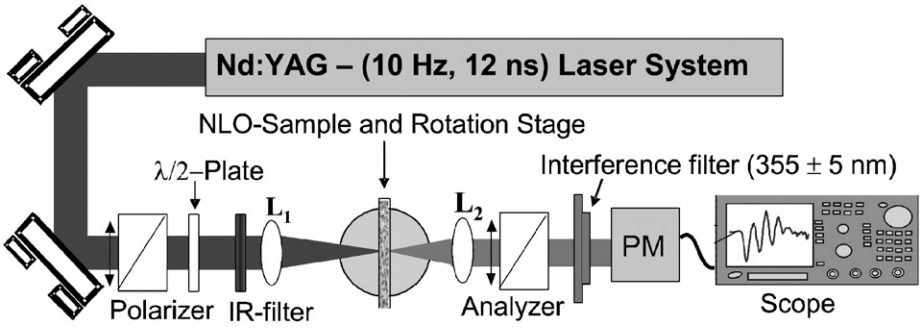

Fig. 2. Experimental device implemented for NLO-THG measurements in Jäger nickel (II)-based thin films.

microscopy as shown in Table 1 and Fig. 3, where 3D micrographs are shown in order to provide a large surface inspection ($20 \times 20\,\mu m$) of the micro-structural arrays, topological structure, porosity and film quality of the deposited layers. In the case of films deposited from the precursor $[Ni(C_{18}H_{28}N_4O_2)](PF_6)_2$, small particles agglomerate to generate huge rounded grains in the range of 0.5–1 μm (measured from amplified high-quality digitized images), showing a reasonably homogeneous distribution at large micrometric length scale (see Fig. 3a). This arrangement shows the largest roughness with considerable inter-grain porosity (see Table 1); here, at least a bimodal grain size distribution can be observed. For $[Ni(C_{17}H_{25}N_4ONH(CH_2)_4NH_2)](PF_6)_2$ (compound 1a) thin-film samples, a dramatic change in the film morphology can be observed, namely the formation of randomly oriented, flattened-like stripe structures, with lengths ranging from 2 to 10-μm and thicknesses in the order of 1-μm taking place (see Fig. 3b). These flattened systems grow unidirectionally, forming very homogeneous and stable arrangements with the smallest roughness; nevertheless, film deposition on the substrate surface is not uniform and microscopic porosity increases substantially. The stripe systems may be produced during deposition due to crystallization of the 1a-compound on the substrate, achieved at the employed substrate temperature and vacuum thermal evaporation conditions. In fact, as shown later in this section, XRD studies reveal a slight degree of crystallinity for this sample which certainly helps towards clarifying this point (see Fig. 4). $[Ni(C_{17}H_{25}N_4ONH(CH_2)_{12}NH_2)](PF_6)_2$ (compound 1b)-based thin films are formed by greater rounded grains compared to those of the precursor compound with dimensions in the order of 2–4 μm (see Fig. 3c); the intergranular space is clearly increased whereas homogeneity and film quality decrease considerably, since several imperfections and dispersed particles can be identified on the film surface; film roughness is almost as high as that of the precursor sample. Finally, deposited thin-film samples from compound $[Ni(C_{17}H_{25}N_4O(C_{14}H_{10}N_2O_2))](PF_6)_2$ (compound 1c) reveal a fully different structure (see Fig. 3d). Indeed, the corresponding morphology becomes smoother with narrower grain-size distribution, smaller grain sizes and inter-grain porosity; agglomeration effects are also reduced and the formation of small and ordered rod-like structures with lengths ranging from 0.5 to 2 μm can be observed. This contributes to an improvement of the film quality obtained for this compound.

Table 1
AFM evaluation of the thin-film roughness

Sample	RMS roughness (A)
$[Ni(C_{18}H_{28}N_4O_2)](PF_6)_2$ (precursor compound)	231
$[Ni(C_{17}H_{25}N_4ONH(CH_2)_4NH_2)](PF_6)_2$ (compound 1a)	17.3
$[Ni(C_{17}H_{25}N_4ONH(CH_2)_{12}NH_2)](PF_6)_2$ (compound 1b)	209
$[Ni(C_{17}H_{25}N_4O(C_{14}H_{10}N_2O_2))](PF_6)_2$ (compound 1c)	125

Fig. 4 shows the XRD patterns of all the studied film samples. The precursor-, 1b- and 1c-thin-film samples exhibit an explicit amorphous structure since no other significant peak-signals besides the characteristic enveloping XRD patterns collaterally obtained from the SiO_2 substrates can be noticed (distinctive XRD pattern of SiO_2: broad XRD-signal with a typical peak centered at 21.985°). Although the XRD pattern measured from the 1a film sample also reveals a predominantly amorphous arrangement, a well-defined XRD-peak signal located at 25.065° can be clearly recognized. This signal suggests the formation of a regular structure in accordance with AFM-studies, which should be analyzed in more detail elsewhere. For the purposes of the present work, it is expected that such structural and morphological variations as observed in the film samples will affect other important physical properties, particularly the optical performance of these molecular systems, as will be shown later in this work.

3.2. FTIR analysis

FTIR spectroscopic measurements on thin films were made to determine if there were significant changes in the

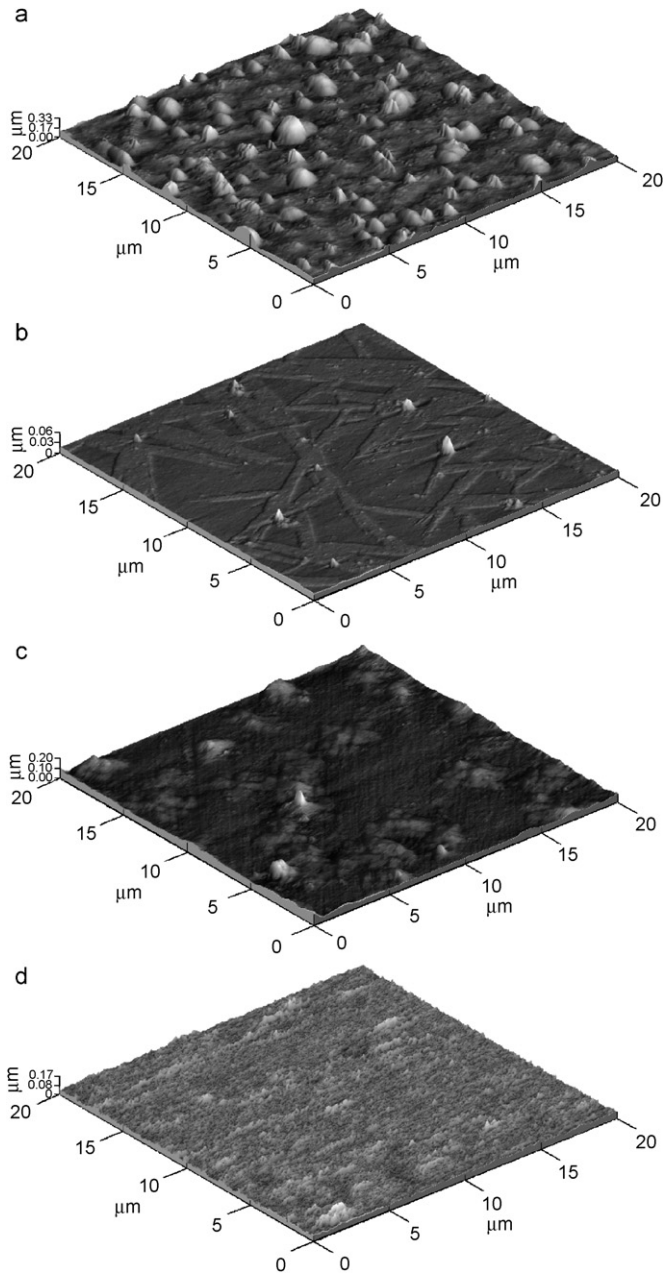

Fig. 3. 3D-micrographs obtained by AFM and showing the surface morphology of thin films deposited on Corning 7059 glass slices from (a) the precursor sample, (b) sample 1a, (c) sample 1b and (d) sample 1c, respectively.

raw materials after thermal evaporation. Table 2 shows the IR band spectra for the newly synthesized compounds in their different forms (powder and film). From the FTIR measurements, it was observed that the deposited materials have the same absorption bands as the synthesized powders, suggesting that the sublimation and deposition processes are of a molecular nature, without significant changes in the relative chemical composition of the materials. Taking into account that the substrate temperature was the same for all depositions (298 K) and that the deposited materials were formed by macromolecular compounds, it can be argued that the molecules impinging

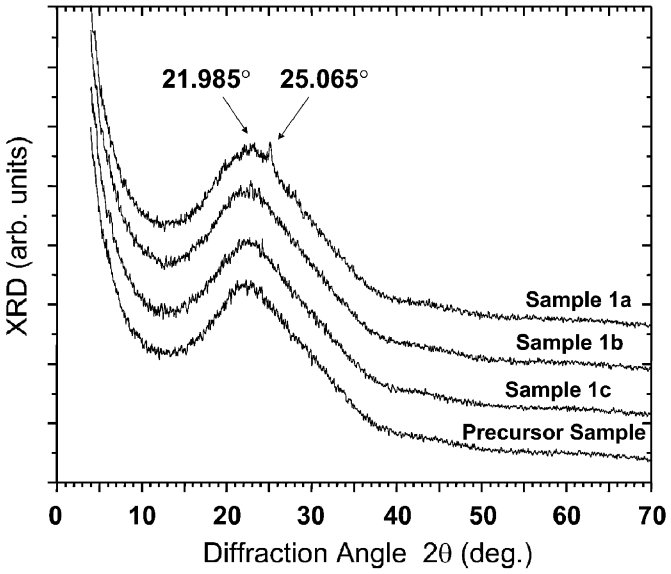

Fig. 4. Comparative XRD patterns recorded in Jäger nickel (II)-based thin-film systems.

on the surface of the substrates do not have enough energy to induce drastic changes in the physical and chemical properties of the deposited material that may be related to the crystalline or amorphous nature of the substrates. There are reports on depositions of different kinds of amorphous and crystalline materials leading to results that are similar to those of the present work [19–21].

As can be seen from Table 2, there are three bands in the IR spectra for the synthesized compounds [22,23]. The first one is related to C═C stretching vibrations at 1625–1630 cm^{-1} and the second band corresponds to C═N vibrations at 1570–1577 cm^{-1}, both related to the nickel macrocycle. The third band is due to N–H vibrations of the amine bounded to the macrocycle occurring at 3395–3405 cm^{-1}. The first two bands show Jäger complex leasing, while the third band proves that the amine is bounded to the macrocycle. According to Kumar and Katovic [24,25], there is an additional band when there are bidentate amines added to the nickel complex, due to the vibration of the amine group of the unbounded tip, appearing between 2923 and 2960 cm^{-1}. The presence of this band indicates that the bidentate amine is bounded to the complex by only one of its tips. This is important because it may occur that an amine of the 1,12-diaminododecane size is bounded to the complex by its two tips from the corresponding leased zones [22,23,26].

3.3. Electric properties

Fig. 5 shows the temperature dependence of the electric current for all studied compounds: $[Ni(C_{17}H_{25}N_4ONH(CH_2)_4NH_2)](PF_6)_2$, $[Ni(C_{17}H_{25}N_4ONH(CH_2)_{12}NH_2)](PF_6)_2$, $[Ni(C_{17}H_{25}N_4O(C_{14}H_{10}N_2O_2))](PF_6)_2$ and the precursor complex from which they were prepared, $[Ni(C_{18}H_{28}N_4O_2)](PF_6)_2$. The variations observed in the magnitude of electric

Table 2
IR data for the reported compounds in powder and thin film (all units cm^{-1})

Compound	ν (C=C)	ν (C=N)	ν (N–H)	ν (NH_2)
$[Ni(C_{17}H_{25}N_4ONH(CH_2)_4NH_2)](PF_6)_2$ (1a powder)	1628	1574	3405	2914
$[Ni(C_{17}H_{25}N_4ONH(CH_2)_4NH_2)](PF_6)_2$ (1a thin film)	1624	1577	3407	2920
$[Ni(C_{17}H_{25}N_4ONH(CH_2)_{12}NH_2)](PF_6)_2$ (1b powder)	1630	1577	3391	2921, 2852
$[Ni(C_{17}H_{25}N_4ONH(CH_2)_{12}NH_2)](PF_6)_2$ (1b thin film)	1630	1571	3386	2921
$[Ni(C_{17}H_{25}N_4ONH(CH_2)_{12}NH_2)](PF_6)_2$ (1c powder)	1631	1557	3405	2942, 2960
$[Ni(C_{17}H_{25}N_4ONH(CH_2)_{12}NH_2)](PF_6)_2$ (1c thin film)	1628	1570	3406	2940, 2958

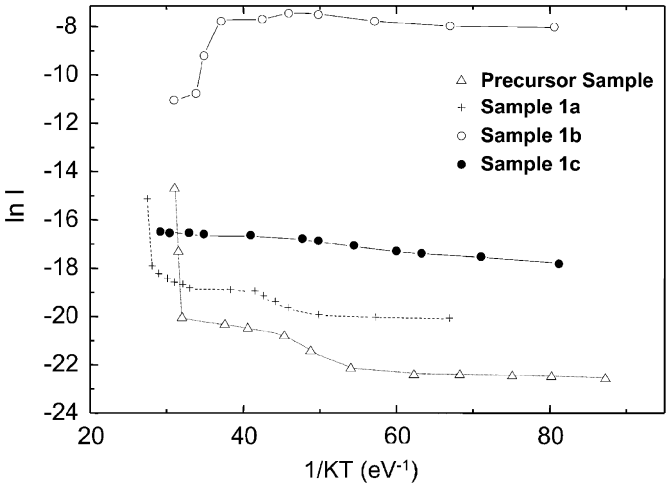

Fig. 5. Temperature-dependent electric current, measured in Jäger nickel (II)-based thin-film systems for (a) the precursor molecular sample: $[Ni(C_{18}H_{28}N_4O_2)](PF_6)_2$, (b) compound 1a: $[Ni(C_{17}H_{25}N_4ONH(CH_2)_4NH_2)](PF_6)_2$, (c) compound 1b: $[Ni(C_{17}H_{25}N_4ONH(CH_2)_{12}NH_2)](PF_6)_2$ and (d) compound 1c: $[Ni(C_{17}H_{25}N_4O(C_{14}H_{10}N_2O_2))](PF_6)_2$.

current may be due to the different amine groups. The 1b compound shows by far the largest electrical current. Nevertheless, its behavior at low temperatures is almost constant; above 288 K this behavior becomes conductor-like, without leading to chemical changes in the compound structure. The rest of the compounds show, for all temperatures, a behaviour corresponding to a semiconductor material. In these materials, compounds with voluminous substitutes and high molecular weights such as 1,12-diaminedodecane (compound 1b) and 2,6-diamineanthraquinone (compound 1c) present the largest current, which certainly make these compounds more interesting regarding their optical properties, as will be shown later.

Taking into account the amorphous nature of the deposited materials, the electrical conductivity was measured only along one direction. The electric conductivity σ of these materials depends on the absolute temperature T as described by

$$\sigma = \sigma_m \exp\left(-\frac{\Delta E_m}{KT}\right), \quad (1)$$

where σ_m is the pre-exponential factor, ΔE_m is the activation energy for electric conductivity, and K is Boltzmann constant. Calculated values of ΔE_m are shown in Table 3. The quantity ΔE_m is an activation energy involving both the energy necessary to excite electrons from the localized states toward extended states through the mobility edge and the electrical conduction by means of the hopping mechanism between localized states. The electric conductivity at 298 K for the synthesized molecular solids and the starting materials was also calculated (see Table 3). All compounds show electrical conductivity values within the reported interval found in the literature for molecular semiconductors (from 10^{-6} to $10^{1}\,\Omega^{-1}\,cm^{-1}$) [27,28]. The $[Ni(C_{17}H_{25}N_4ONH(CH_2)_{12}NH_2)](PF_6)_2$ (compound 1b) material is the one which presents the largest electrical conductivity at room temperature. The corresponding AFM image shows that the deposited material is formed by large rounded grains, and that the intergranular space increases in comparison with that of the precursor material (see Fig. 3c). However, this fact does not mean that the intergranular space is free of deposited material, as can be clearly recognized by a careful inspection of Fig. 3. The thin film deposited onto the surface of the substrate is uniform and the large grains arise from agglomeration effects. We believe that the extremely thin layer deposited in a wide area of the substrate interface could form low electrical-resistance pathways permitting the flow of electric current and resulting in the largest electrical conductivity. Nevertheless, it may occur that the amine 1,12-diaminododecane be bounded to the complex by its two tips not leaving dangling bonds. The dangling bonds may act as charge carrier traps leading to an increment in the electrical resistance of the material. According to Morales et al., the conductivity properties of DADMTNi-TCNQ complexes are basically related to the planarity of their own constitutive molecules, to the presence of delocalized π-electrons, and to the presence of a transition-metallic ion [29,30]. Apparently, charge transport in these materials occurs through the Ni (II) ions. On the other hand, compounds with voluminous amines and high molecular weights present the largest conductivity for these materials. In these materials, conductivity may be explained in two stages, which are distinguished from curves I vs $1/KT$ (see Fig. 5) for these compounds: (i) at high temperatures, conductivity is achieved because thermal energy is large enough to excite electrons from the extended sates into the

Table 3
Thin-film activation energy, electrical conductivity at 20 °C (100 V) in the ohmic regime and film thickness

Compound	Activation energy ΔE_m (eV)	Electrical conductivity in thin films, σ ($\Omega^{-1}cm^{-1}$)	Thin-film thickness, (nm)
$[Ni(C_{18}H_{28}N_4O_2)](PF_6)_2$ (precursor compound)	0.109	4.3 E−6	182
$[Ni(C_{17}H_{25}N_4ONH(CH_2)_4NH_2)](PF_6)_2$ (compound 1a)	0.468	7.2 E−6	150
$[Ni(C_{17}H_{25}N_4ONH(CH_2)_{12}NH_2)](PF_6)_2$ (compound 1b)	0.156	0.151	67
$[Ni(C_{17}H_{25}N_4O(C_{14}H_{10}N_2O_2))](PF_6)_2$ (compound 1c)	0.08	8.2E−5	130

conduction band. Conductivity will be due to the motion of electrons in the electric field. (ii) In the second stage, namely thermally assisted jump, which occurs at lower temperatures, electrons in localized states may contribute to conductivity only if they acquire enough energy to hop from one localized state to another.

3.4. Linear and non-linear optical properties

The optical absorbance spectra of the studied compounds and the precursor structure in thin films deposited on Corning 7059 glass slices were recorded from 200 to 1100 nm and are shown in Fig. 6. The thickness of the deposited films varies from 67 to 182 nm (see Table 3); hence the Beer–Lambert law applies for such semi-transparent thin-film systems. It is evident from Fig. 6 that these compounds have well defined and different physical properties depending on their molecular structure. In general, the weak absorption displayed by all samples within the visible-near infrared (VIS-NIR) range, make these molecular systems attractive candidates for optical applications due to their adequate transparency at optical wavelengths (see Fig. 6a). In contrast, higher absorption is detected in the UV region with an absorption peak consistently appearing around 240 nm for all samples; this huge absorption band is probably produced by the glass substrates.

The main differences observed in the absorption spectra of the molecular systems under study are better appreciated within the 300–500 nm interval (see Fig. 6b), where the precursor sample $[Ni(C_{18}H_{28}N_4O_2)](PF_6)_2$ exhibits low absorption, showing a weak absorption band around 385 nm.Compound $[Ni(C_{17}H_{25}N_4ONH(CH_2)_4NH_2)](PF_6)_2$ (1a) exhibits the lowest absorption, showing a smooth and monotonically decreasing behavior. Similarly, compound $[Ni(C_{17}H_{25}N_4ONH(CH_2)_{12}NH_2)](PF_6)_2$ (1b) shows a slightly larger absorption in the same spectral range with the same functional dependence as compound (1a). By contrast, compound $[Ni(C_{17}H_{25}N_4O(C_{14}H_{10}N_2O_2))](PF_6)_2$ (1c) exhibits the strongest optical absorption with a fully different functional dependence. In this case, two well-defined absorption bands centered at 331 and 405 nm can be easily recognized. Due to its well-defined shape and stronger intensity, the last band cannot be considered a red-shifted band related to the 385 nm band from the precursor sample. Differences on the relative absorption intensities of the studied structures arise also from the diverse grain densities observed by AFM-micrographs (see Fig. 3), where maximal absorption was found for the

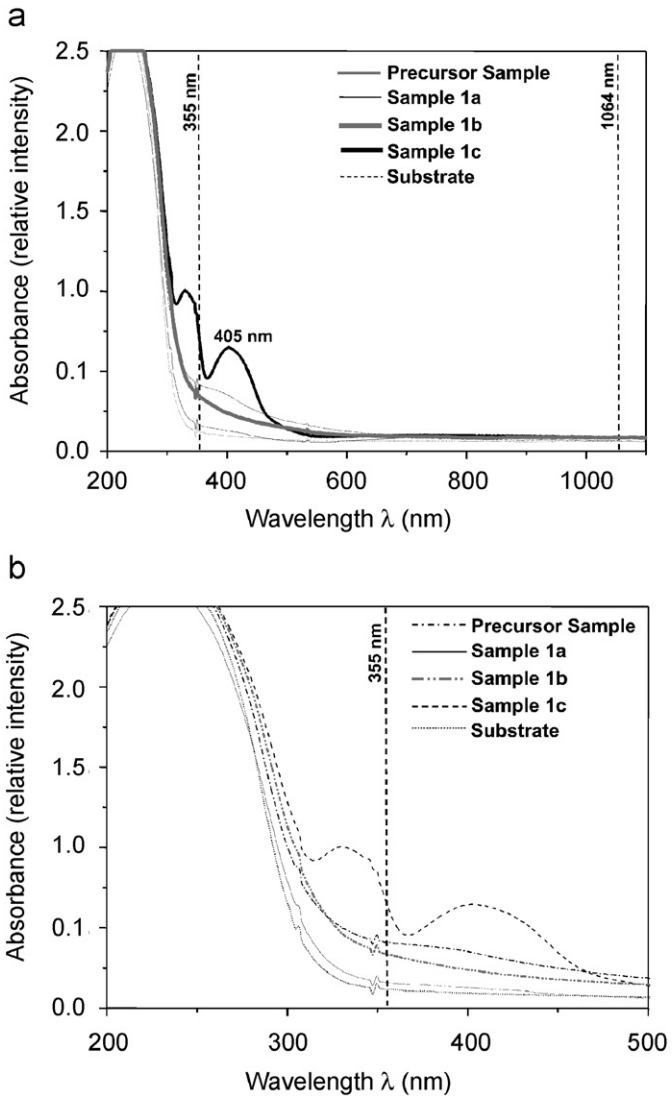

Fig. 6. (a) Comparative absorption spectra recorded in Jäger nickel (II)-based thin-film systems, recorded from 200 to 1100 nm, and (b) comparative absorption spectra recorded from 200 to 500 nm (detail).

densely packed 1c-based thin-film structure, followed by the precursor and the 1b samples. Furthermore, it is observed that the positions of the absorption bands are poorly influenced by the backbone structure of these compounds and their precursor. Finally, the wide and non-negligible absorption band exhibited by the 1b-molecular system (for $\lambda = 400$–500 nm) and by compound 1c within the visible region (centered at $\lambda = 405$ nm) may suggest a major conjugation degree of delocalized π-electrons compared to the other samples, which only exhibit minor absorption tails from this value on. This last possibility was explored in a series of NLO-THG experiments as discussed below. In this context, the available laser excitation line (at $\lambda_\omega = 1064$ nm) and the line at the THG wavelength ($\lambda_{2\omega} = 355$ nm) are also depicted in Fig. 6. At these wavelengths, low-absorption experimental conditions occur, allowing non-resonant conditions for cubic NLO-characterization.

The width of the optical band gap (E_g) can be approximated from a straight-line fit in the $(\alpha h\nu)^{1/2}$ versus $(h\nu)$ plot. The absorption coefficient α near the band edge in many amorphous semiconductors shows a potential dependence on photon energy usually obeying the empirical relation [21]:

$$\alpha h\nu = \beta (h\nu - E_g)^n, \tag{2}$$

where β^{-1} is the band edge parameter, n is a number characterizing the transition process which takes values $\frac{1}{2}$, 1, 2 or $\frac{3}{2}$, depending on the nature of the electronic transitions responsible for the absorption [31]. In amorphous semiconductors, the optical transitions are dominated, to a first approximation, by the so-called non-direct transitions. In these electronic transitions, from states in the valence band to states in the conduction band, there is no conservation of the electronic momentum [32]. Fig. 7 shows the $(\alpha h\nu)^{1/2}$ versus $(h\nu)$ plot for the considered thin films. The band gap values of : $[Ni(C_{17}H_{25}N_4ONH(CH_2)_4NH_2)](PF_6)_2$ (1a), $[Ni(C_{17}H_{25}N_4ONH(CH_2)_{12}NH_2)](PF_6)_2$ (1b), $[Ni(C_{17}H_{25}N_4O(C_{14}H_{10}N_2O_2))](PF_6)_2$ (1c) and the precursor complex thin films were found to be 1.6, 2.0, 1.5 and 1.5 eV, respectively.

PL measurements were carried out at room temperature and atmospheric pressure on the same films deposited on Corning 7059 glass slices (excitation wavelength line was set to $\lambda_{ex} = 250$ nm) and the PL-spectra were recorded from 250 to 700 nm as it is shown in Fig. 8. Based on the fluorescence spectra obtained from the precursor and a Corning 7059 glass substrate (not shown here), we consider that the resultant spectra of compounds 1a, 1b and 1c are constituted from the following PL-peak signals: 296, 376, 397, 451, 469, 544, and 584 nm. The bands centered at 296, 469 and 584 nm remain nearly unchanged and show strong signals, whereas all the other PL peaks gradually disappear within the PL-spectra of compounds 1a, 1b and 1c. In the present experiments, the highest PL-emissions were recorded within the 380-530 nm spectral range for all the studied samples. The largest PL-intensity was obtained

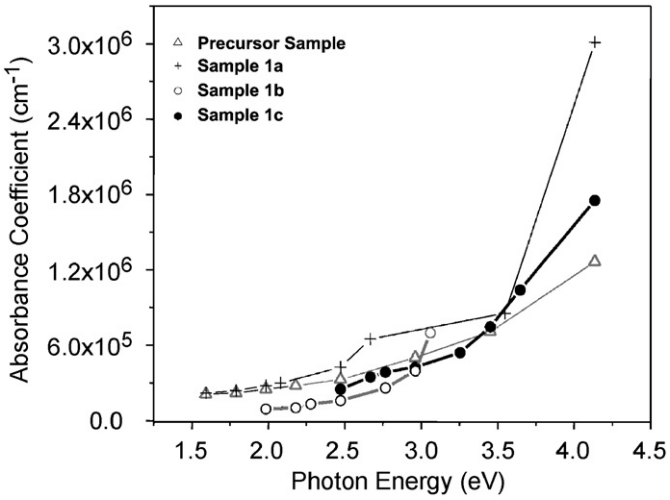

Fig. 7. Dependence of $(\alpha h\nu)^{1/2}$ as a function of the photon energy $h\nu$ for thin films grown from: (a) the precursor molecular sample: $[Ni(C_{18}H_{28}N_4O_2)](PF_6)_2$, (b) compound 1a: $[Ni(C_{17}H_{25}N_4ONH(CH_2)_4NH_2)](PF_6)_2$, (c) compound 1b: $[Ni(C_{17}H_{25}N_4ONH(CH_2)_{12}NH_2)](PF_6)_2$ and (d) compound 1c: $[Ni(C_{17}H_{25}N_4O(C_{14}H_{10}N_2O_2))](PF_6)_2$.

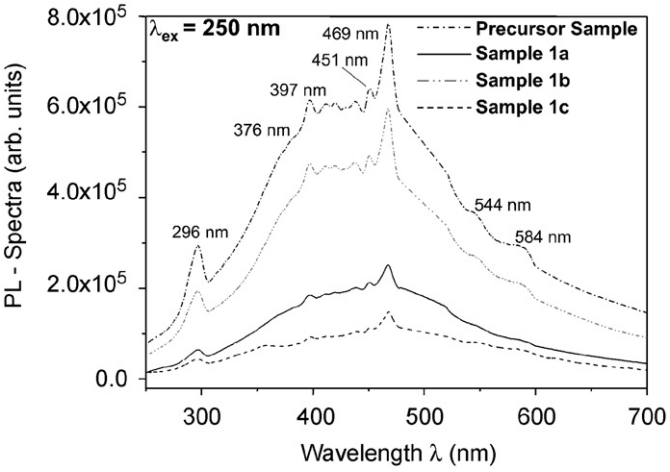

Fig. 8. Comparative PL spectra recorded in Jäger nickel (II)-based thin-film systems, from 250 to 700 nm ($\lambda_{ex} = 250$ nm).

from the precursor sample, followed by the emissions measured from samples 1b, 1a and 1c, respectively. Samples 1b and 1c show the most interesting absorbance profiles from the optical point of view (see Fig. 6). We hypothesize that the non-negligible absorption bands observed in the 400–500 nm spectral range for the 1b and 1c-based thin-film samples may lead to a sharp decrease in the PL-emission (especially so in the case of compound 1c) within this interval due to self-absorption effects induced by the high conjugation degree of this compound. Nevertheless, according to Table 3, the 1b-based thin-film sample is much thinner compared to the 1c-based film and exhibits lower absorption. As this compound has the strongest PL-spectra among the three newly synthesized compounds, it suggests a complex multi-level electronic structure, suitable

for cubic NLO effects like THG. The latter hypothesis was explored by means of NLO-measurements as reported below.

In order to investigate the NLO properties of Jäger-type molecular systems, second and third harmonic optical generation (SHG and THG) experiments were performed with these complexes. Since quadratic $\chi^{(2)}$-NLO properties were not detected by means of SHG experiments and non-centrosymmetric crystalline structures of these materials are required in order to obtain measurable $\chi^{(2)}$-coefficients, it is confirmed that all studied structures primarily exhibit an amorphous organization (in case of compound 1a, polycrystalline centrosymmetric arrangements may yet be possible, lacking in any case a SHG response). The cubic $\chi^{(3)}$-NLO-properties were also investigated by means of the optical THG-technique to account for amorphous and crystalline centrosymmetric material structures. Experimental single beam techniques based on THG give direct access to the complex value of the non-degenerate $\chi^{(3)}(-3\omega, \omega, \omega, \omega)$ cubic non-linear coefficient, which can also be related to the degenerate $\chi^{(3)}(-\omega; \omega,-\omega, \omega)$ component in order to give a good estimate of the relevant intensity-dependent non-linear refractive index (IDRI or n_2): $\mathrm{Re}(\chi^{(3)}(-\omega, \omega,-\omega, \omega)$ [33], which is usually determined by Z-scan experiments [34,35]. An advantage of the THG-technique is the fact that the THG response accounts only for the ultra-fast electronic response, so that vibrational, orientational, and thermal effects, which may contribute to the overall NLO response of the material, are excluded.

Fig. 9 shows the calibrated NLO $\chi^{(3)}$- coefficients of the thin-film samples under study according to their Maker-fringes patterns. Fig. 9a shows the typical Maker-fringes patterns (front-configuration, P/In–P/Out polarizing geometry and non-resonant configuration at $\lambda_\omega = 1064\,\mathrm{nm}$ and $\lambda_{3\omega}{\sim}355\,\mathrm{nm}$) of the precursor, 1a, 1b and 1c thin-film samples deposited on 1mm thick Corning 7059 glass slices compared with the fringes pattern generated by the substrate alone. The Maker-fringes patterns of the molecular film-plus-substrate systems do not show a significant oscillating dependence with increasing incident angles when compared to the fringes measured for the reference substrate. On the other hand, these fringes are clearly more intense than those recorded for the substrate alone, so the lack of sharp multi-oscillations may be due to the fact that the thickness of the studied films is smaller than their characteristic coherence lengths (usually in the range of a few microns) and thus the THG-intensity will not longer follow the phase-matching-dependent oscillations with the medium thickness. Nevertheless, the THG-response obtained at normal incidence gives the highest conversion efficiency (“first” phase-matching condition satisfied), which permits the relative evaluation of the $\chi^{(3)}$ coefficients. According to D’Amore et al. and Nakanishi et al. [14,36], due to our nearly non-resonant experimental conditions, in which the fundamental and free waves are weakly absorbed by the Jäger-based thin-film molecular systems (see Fig. 6), the determination of the non-

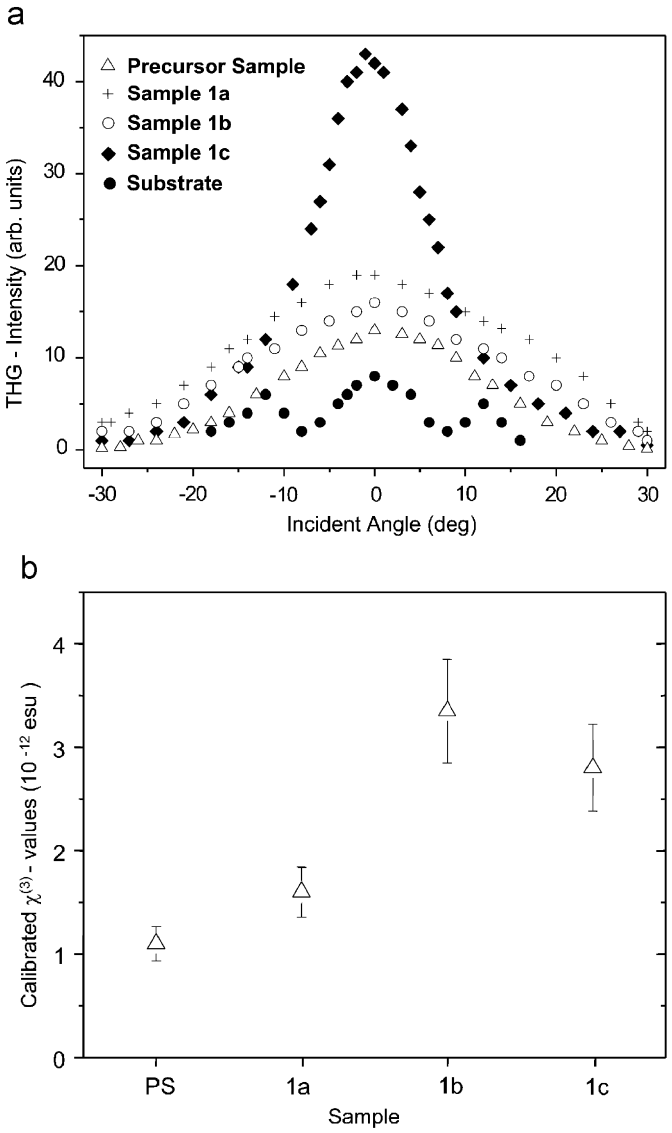

Fig. 9. (a) Angle dependent THG-measurement performed in Jäger nickel (II)-based thin-film systems (Maker-fringes experiment, monolayer system). Measurements were performed by implementing the P-In/P-Out polarizing geometry. (b) Relative calibration performed according to Ec. 3 of the text, to obtain the $\chi^{(3)}(-3\omega, \omega, \omega, \omega)$ NLO-coefficients.

degenerate $\chi^{(3)}(-3\omega, \omega, \omega, \omega)$ values can be approximated by the following expression:

$$\chi^{(3)-\mathrm{Film}} \propto \chi^{(3)-\mathrm{Substrate}} \left(\frac{2l_c^{\mathrm{Substrate}}}{\pi l_{\mathrm{Film}}}\right)\left(\frac{I_{3\omega}^{\mathrm{Film}}}{I_{3\omega}^{\mathrm{Substrate}}}\right)^{1/2}, \qquad (3)$$

where $l_c^{\mathrm{Substrate}}$ represents the coherence length of the substrate (~8 μm at $\lambda_\omega = 1064\,\mathrm{nm}$), and $\chi^{(3)-\mathrm{Film}}$ and $\chi^{(3)-\mathrm{Substrate}}$ are, respectively, the values of the cubic non-linear coefficients of the Jäger-based thin-film samples and the Corning 7059 glass slices (previously calibrated by means of the fused silica reference plate), while $I_{3\omega}^{\mathrm{Film}}$ and $I_{3\omega}^{\mathrm{Substrate}}$ are the peak intensities of the *Maker*-fringes patterns of both the thin-film sample and the substrate alone.

In principle, both the film and the substrate contribute to the detected THG-signal (as the focal length of the focusing lens is less than 50 mm in order to make the air contribution to the THG-signal negligible [14,36,37]); these two contributions must be separately identified in order to give a good estimate of the $\chi^{(3)-\mathrm{Film}}$ coefficients. Moreover, since the film is deposited only on one side of the substrate, the experimental configuration is asymmetric from a geometrical view point and different relations have been developed in order to, respectively, fit the 'front' configuration, where the fundamental beam enters first through the film, or the 'back' configuration, where the films stay behind the substrate. The equations for the interpretation of Maker-fringes experimental patterns have been derived by several authors [14,15,17,36–41]. Under this framework, Fig. 9b shows the $\chi^{(3)-\mathrm{Film}}$ calibrated coefficients according to Eq. (3) (note that small variations in the film thickness may induce a drastic variation on the calibrated $\chi^{(3)-\mathrm{Film}}$ values according to this formula); hence the highest cubic NLO coefficient was found for the 1b based thin film sample, with value $\chi^{(3)}_{1b-\mathrm{Film}} = 3.35 \times 10^{-12}$ esu ($= 4.65 \times 10^{-20}\,\mathrm{m^2\,V^{-2}}$), followed by the 1c-based thin film. A substantial decrease of the $\chi^{(3)-\mathrm{Film}}$ value occurs for sample 1a, which is only slightly larger than that measured for the precursor sample; the reference substrate exhibits the lowest cubic NLO coefficient (not shown for simplicity on the graph scale).

It was verified that the diverse molecular systems obtained from the precursor sample had notable differences in their linear and non-linear optical properties. The cubic NLO effects in particular were considerably improved for compounds 1b and 1c, which exhibited higher conjugation degree, low optical absorption and adequate electronic multi-level organizations, which were sensitively detected by NLO-THG measurements. In addition to the distinctive differences produced by the diverse chemical structures on the THG responses and to the straight correlation attributed to the thin-film thickness (see Eq. (3)), the film structure and variations of the grain size distribution could play an important role concerning the origin and magnitude of the observed THG-signals. Here, assuming a high correlation between the film structure and the NLO response, and considering the greater number of grain boundaries or interfaces observed in the 1c sample, where the grain size is smaller, there may be a vast number of dangling bonds at the interfaces resulting in extra carriers or defects in the film. This is of considerable interest, as it has been demonstrated that higher carrier densities and defects can enhance the non-linearity of crystals [42,43]. In the case of compound 1b, its higher conductivity and delocalization explains the intense cubic NLO-phenomena.

4. Conclusions

Semiconductor materials from nickel (II) Jäger compounds and from the bidentate amines—1,4-diaminebutane, 1,12-diaminedodecane and 2,6-diamineanthraquinone were synthesized. Thin films of these materials were deposited by vacuum thermal evaporation. They were formed by the same chemical units as those of the corresponding synthesized powders. The thermal evaporation process did not appreciably change intra-molecular bonding, suggesting that the deposition process can be, in general, considered a molecular process and the substrate temperature is not high enough to provide the surface mobility necessary for the molecular units to produce highly ordered crystalline films. XRD measurements confirm this supposition, in spite of compound 1a showing a stronger tendency to form crystalline structures; this interesting fact should yet be investigated in further detail. From the electric current values, it is clear that all the molecular thin films show a semiconductor-like behavior after evaporation, with conductivities in the order of 10^{-6}–$10^{-1}\,\Omega^{-1}\,\mathrm{cm}^{-1}$ at room temperature. It was also found that the temperature-dependent electric current is always higher for the voluminous amines with large molecular weights. The value of the calculated activation energies, the order of magnitude of the electrical conductivities and the feasibility of preparing thin films from these materials suggest that it may be possible to use them in the preparation of nanoelectronic devices.

Thin-film morphology inspections performed by AFM showed wide structural variations among the studied samples—higher film quality (high homogeneity, good micro-structured grain-size distribution and high density)—were obtained for the precursor and the 1c-based samples, whereas samples obtained from compound 1a exhibited a dramatic change in the film morphology, forming randomly oriented flattened-like stripe structures with high inter-structural porosity, which apparently result from a low degree of crystallization of this compound on the substrate, this issue should be further investigated in order to determine convenient parameters for film deposition. Compound 1b exhibited a wider and larger grain-size distribution; the intergranular space was clearly increased whereas homogeneity and film quality decreased significantly. Besides the intrinsic chemical differences between the studied systems, such structural variation as observed in the molecular film arrangements provoked as well a notable influence on the optical properties of these compounds. In this sense, thin films produced from the 1c- and 1b-molecular structures exhibited a larger conjugation degree of the delocalized π-electron system, which in combination with a high conductivity (sample 1b) or a highly ordered, densely packed film structure with small grain size distribution (sample 1c), allowed the most favorable conditions to generate cubic NLO-effects like THG. The measurement of only-cubic, non-degenerated $\chi^{(3)}(-3\omega,\ \omega,\ \omega,\ \omega)$ NLO coefficients in all the studied samples, instead of quadratic-$\chi^{(2)}$ ones, pointed out to predominantly amorphous structured-molecular arrangements, also shown by XRD experiments. The cubic NLO effects were substantially enhanced for compound 1c and particularly for compound 1b with respect to the precursor

sample, where $\chi^{(3)}(-3\omega, \omega, \omega, \omega)$ values in the promising range of 10^{-12} esu (10^{-20} m^2 V^{-2}) have been evaluated.

The experimental results reported in this paper have been primarily carried out as a step towards the understanding of the complex Jäger-based compounds developed in this work, where qualitative and then quantitative physical analysis were performed in order to explore their potential for the development of semiconductor, optoelectronic and NLO devices, and as a practical alternative to expensive, inorganic monocrystalline materials. This is especially interesting for this kind of materials, given that their high optical quality (adequate transparency within the visible spectral region), together with their semiconductor properties, makes them interesting candidates to fulfill requirements demanded in high-tech applications. Nevertheless, further studies and improvements in the deposition of these thin-film structures, in their quality, in the optimization of the vacuum thermal evaporation parameters and in the electrical and NLO-responses will be necessary. Such investigations are currently underway.

Acknowledgments

The authors wish to thank the technical assistance of José G. Bañuelos (CCADET-UNAM), José Ramón Alvarez Bada (ITESM-CCM) and Leticia Baños (IIM-UNAM). O. G. Morales-Saavedra gratefully acknowledges the financial support from SEP-CONACYT-México (grant: 47421), and from the DAAD academic organization (Germany).

References

[1] F.L. Carter, R.E. Siatokowski, H. Wohltjen, Molecular Electronic Devices, North-Holland, New York, 1988.

[2] J. Puigdollers, C. Voz, A. Orpella, I. Martin, M. Vetter, R. Alcubilla, Pentacene thin-films obtained by thermal evaporation in high vacuum, Thin Solid Films 427 (2003) 367–370.

[3] P.N. Prasad, D.J. Williams, Introduction to Nonlinear Optical Effects in Molecules and Polymers, Wiley Interscience, New York, 1991 Chapter 1.

[4] D. De Caro, H. Alves, M. Almeida, S. Caillieux, M. Elgaddari, C. Faulman, I. Malfant, F. Senocq, J. Fraxedas, A. Zwick, L. Valade, Conducting oriented-$[(n\text{-}C_4H_9)_4N]_2[Ni(dcbdt)_2]_5$ and new (BEDT-TTF)$[Ni(dcbdt)_2]$ phases as microcrystalline films, electrodeposited on silicon substrates, J. Mater. Chem. 14 (2004) 2801–2805.

[5] L. Pillia, I. Malfant, D. de Caro, F. Senocq, A. Zwick, L. Valade, Conductive thin-films of θ-$(BETS)_4[Fe(CN)_5NO]$ on silicon electrodes—new perspectives on charge transfer salts, New. J. Chem. 28 (2004) 52–55.

[6] D. de Caro, J. Graxedas, C. Faulmann, I. Malfant, J. Milon, J.F. Lamere, V. Colliere, L. Valade, Metallic Thin Films of TTF$[Ni(dmit)_2]_2$ by Electrodeposition on (0 0 1)-Oriented Silicon Substrates, Adv. Mater. 16 (9–10) (2004) 835–838.

[7] S. Caillieux, D. de Caro, L. Valade, M. Basso-Bert, C. Faulmann, I. Malfant, H. Casellas, L. Ouahuab, J. Fraxedas, A. Zwick, Tetrathiafulvalene-based conducting deposits on silicon substrates, J. Mater. Chem. 13 (2003) 2931–2936.

[8] P. Cassoux, D. De Caro, L. Valade, H. Casellas, B. Daffos, M.E. Sánchez Vergara, From molecule-based (super) conductors to thin films, nanowires and nanorings, Mol. Cryst. Liq. Cryst. 380 (2002) 45–52.

[9] F. Kajzar, J.D. Swalen (Eds.), Organic Thin Films for Waveguiding Nonlinear Optics, vol. 11, Gordon and Breach, San Jose, 1996 Chapters. 8–9.

[10] K. Akamatsu, S. Takei, M. Mizuhata, A. Kajinami, S. Deki., S. Takeoka, M. Fujii, S. Hayashi, K. Yamamoto, Preparation and characterization of polymer thin films containing silver and silver sulfide nanoparticles, Thin Solid Films 359 (2000) 55–60.

[11] P.W.R. Corfield, J.D. Mokren, C.J. Hipp, D.H. Busch. Alkoxyethylidene functions as reactive sites for the attachment of pendent groups to complexes of macrocyclic ligands. Crystal structure and reactivity patterns. J. Am. Chem. Soc. 95 (13) (1973) 4465–4466.

[12] R. Boyd, Nonlinear Optics, Academic Press, San Diego, 1992 Chapter 2.

[13] P.D. Maker, R.W. Terhune, M. Nisenoff, C.M. Savage, Effects of dispersion and focusing on the production of optical harmonics, Phys. Rev. Lett. 8 (1962) 21–23.

[14] F. D'Amore, A. Zappettini, G. Facchini, S.M. Pietralunga, M. Martinelli, C. Dell'Erba, C. Cuniberti, D. Comoretto, G. Dellepiane, Third order optical characterization of a π-conjugated polydiacetylene by Maker fringes technique, Synth. Met. 127 (2002) 143–146.

[15] F. D'Amore, M. Di Giulio, S.M. Pietralunga, A. Zappettini, L. Nasi, V. Rigato, M. Martinelli, Sputtered stoichiometric TeO_2 glass films: dispersion of linear and nonlinear optical properties, J. Appl. Phys. 94 (2003) 1654–1661.

[16] S.R. Marder, J.E. Sohn, G.D. Stucky, Materials for nonlinear optics, chemical perspectives, in: ACS Symposium Series, vol. 455, American Chemical Society, Washington, DC, 1991. (Chapter 4).

[17] F. Kajzar, J. Messier, Third-harmonic generation in liquids, Phys. Rev. A 32 (1985) 2352–2363.

[18] H.S. Nalwa, S. Miyata, (Eds.), Nonlinear optics of organic molecules, first ed., CRC Press, Boca Raton, Florida, 1997 (Chapter 11).

[19] J. Fandiño, A. Ortiz, L. Rodríguez-Fernandez, J.C. Alonso, Composition, structural and electrical properties of fluorinated silicon nitride thin films grow by RPECVD from SiF_4/NH_3 mixtures, J. Vac. Sci. Technol. A 22 (2004) 570–577.

[20] A. Ortiz, J.C. Alonso, E. Haro-Poniatowski, Spray deposition and characterization of zirconium oxide thin films, J. Electron. Mater. 34 (2005) 150–155.

[21] M.E. Sánchez Vergara, A. Ortiz, C. Alvarez Toledano, J.R. Alvarez, Preparation and characterization of molecular material thin films containing diaqua tetrabenzo (b,f,j,n) {1,5,9,13} tetraazacyclohexadecine copper (II) and nickel (II) Bisanthraflavates, Thin Solid Films 488 (2005) 34–39.

[22] M. Buda, J.-C. Moutet, A. Pailleret, E. Saint-Aman, R. Ziessel, Electrosynthesis and coordination chemistry of poly(ferrocene-bipyridyl) fims, J. Electroanal. Chem. 484 (2000) 164–171.

[23] D.H. Busch, Multiple structures from a macrobycyclization reaction. The rich chemistry of the jäger macrocycles, J. Pure Appl. Chem. 52 (1980) 2477–2484.

[24] S. Kumar, R. Malhotra, K.S. Dhindsa, Nucleophilic addition reactions involving the copper (II) complex of tetrabenzo [b, R, j, n] tetraza-cyclohexadecine (2,3; 6,7; 10,11; 14,15 -BZO_4 [16] octane- 1 ,5, 9, 13-N_4), Polyhedron 11 (1992) 1383–1385.

[25] L. Katovic, T. Taylor D. Busch, Nickel (II) and copper (II) complexes containing new monocylic and policyclic hgands derives from the ciclotetrameric Schiff Base of O-aminobenzaldehyde, Inorg. Chem. 3 (1971) 458–462.

[26] B. Korybut-Daszkiewicz, M. Kojina, J.H. Cameron, M. Herron, M.Y. Chavan, A.J. Jircitano, B.K. Coltrain, G.L. Neer, N.W. Alcoock, D.H. Busch, Synthesis and Characterization of Multiply Substituted Lacunar Macrobycyclic Complexes of Nickel (II), a representative crystal structure and preparation of corresponding free ligands, Inorg. Chem. 23 (1984) 903–914.

[27] J. Simon, F. Tournillac, Molecular materials II. Towards electronics finalities, New J. Chem. 11 (1997) 383–399.
[28] J. Simon, Mise au point. Molecular Materials I. Generalities,, New J. Chem. 10 (1986) 295–311.
[29] M.E. Lopez Morales, M. Soriano García, J. Gomez Lara, R.A. Toscano, Physical properties, electrical conductivity and crystal structure of the DADMTANi-TCNQ Complex, Mol. Cryst. Liq. Cryst. 125 (1985) 421–427.
[30] J. Metz, M. Hanack, Synthesis, Characterization and Conductivity of (μ-cyano.)phthalocyaniato) cobalt (III), J. Am. Chem. Soc. 105 (1983) 828–830.
[31] S. Adachi, Optical properties of crystalline and amorphous semiconductors, Kluwer Academic Publishers, Boston, 1999.
[32] G.D. Cody, in: J.I. Pankove (Ed.), Hydrogenated Amorphous Silicon, Part B, Optical Properties, Semiconductors and Semimetals, vol. 21, Academic Press, Orlando, 1984.
[33] F.C. Bloom, A. Driessen, H.J.W.M. Hoekstra, J.B.P. van Schoot, Th.J.A. Poma, Third harmonic generation as a rapid selection tool for organic materials for nonlinear integrated optics devices, Opt. Mater. 12 (1999) 327–331.
[34] M. Sheik-Bahae, A.A. Said, E. Van Stryland, High-sensitivity, single-beam n_2 measurements, Opt. Lett. 14 (1989) 955–957.
[35] M. Sheik-Bahae, A.A. Said, T.H. Wei, D.J. Hagan, E. Van Stryland, Sensitive measurement of optical nonlinearities using a single beam, IEEE J. Quantum Electron. 26 (1990) 760–769.
[36] H. Nakanishi, H. Matsuda, S. Okada, M. Kato, Evaluation of nonlinear optical susceptibility of polydiacetylenes by third harmonic generation, Polym. Adv. Technol. 1 (1990) 75–79.
[37] B. Buchalter, G.R. Meredith, Third order optical susceptibility of glasses determined by third harmonic generation, Appl. Opt. 21 (1982) 3221–3224.
[38] G.R. Meredith, Cascading in optical third harmonic generation by crystalline quartz, Phys. Rev. B 24 (1981) 5522–5532.
[39] X.H. Wang, D.P. West, N.B. McKoewn, T.A. King, Determining the cubic susceptibility $\chi^{(3)}$ of films or glasses by the Maker fringe method: a representative study of spin-coated films of copper phthalocyanine derivation, J. Opt. Soc. Am. B 15 (1998) 1895–1903.
[40] K. Miyano, T. Nishiwaki, A. Tomioka, A simple and accurate method to determine the third-order nonlinear susceptibility of thin films, Opt. Commun. 91 (1992) 501–508.
[41] D.S. Bethune, Optical harmonic generation and mixing in multilayer media: analysis using optical transfer matrix techniques, J. Opt. Soc. Am. B 6 (1989) 910–916.
[42] J. Khaled, T. Fujiwara, M. Ohama, A.J. Ikushima, Generation of second harmonics in Ge-doped SiO_2 thin films by ultraviolet irradiation under poling electric field, J. Appl. Phys. 87 (2000) 2137–2141.
[43] U. Neuman, R. Grunwald, U. Griebener, G. Steinmeyer, W. Seeber, Second-harmonic efficiency of ZnO nanolayers, Appl. Phys. Lett. 84 (2004) 170–172.